VNU Journal of Science: Mathematics - Physics

Journal homepage: https://js.vnu.edu.vn/MaP

Original Article

Spectroscopic Characteristics of Dual - Color CdSe/CdS/$CdSe_{1-x}S_x$/CdS Quantum Dot - Quantum Wells

Le Anh Thi[1], Nguyen Dieu Linh[2], Le Duc Huy[3], Nguyen Thi Thuy Lieu[4], Nguyen Thi Minh Hien[3], Nguyen Xuan Nghia[3,*]

[1]*Institute of Research and Development, Duy Tan University, 3 Quang Trung, Danang, Vietnam*

[2]*University of Science and Technology of Hanoi, 18 Hoang Quoc Viet, Cau Giay, Hanoi, Vietnam*

[3]*Vietnam Academy of Science and Technology, 18 Hoang Quoc Viet, Cau Giay Hanoi, Vietnam*

[4]*Posts and Telecommunications Institute of Technology, Km 10 Nguyen Trai, Hanoi, Vietnam*

Received 12 August 2022
Revised 21 August 2022; Accepted 21 August 2022

Abstract: In this work, preparation and spectroscopic characteristics of CdSe/CdS/$CdSe_{1-x}S_x$/CdS core/shell 1/well/shell 2 structure were presented. The obtained quantum dot - quantum well (QDQW) samples exhibited two emission peaks at 1.97 and 2.2 eV. Excitation power dependent photoluminescence (PL) of the QDQWs indicated that the integrated emission intensities of these peaks increase linearly with excitation power densities up to 1.3×10^2 mW/cm^2. The temperature dependence of the bandgap energies of the QDQW's core and well layer was well described using the Varshni expression. Evidence of the existence of "local wells" in the QDQW's well layer that leads to a more significant change in the maximum position and full width at half maximum of the well's emission peak compared to the core's counterpart was discovered. Annealing samples resulted in the considerable increase of the well layer's emission efficiency.

Keywords: Quantum dot - quantum wells, dual - color, spectroscopic characteristics.

1. Introduction

Dual-color emission semiconductor nanocrystals (NCs) have attracted much attention for many different applications [1-3]. As known, the intensity ratio of the emission bands has been demonstrated to be dependent on factors of the surrounding media such as the pH [4-6], gas pressure [7], and solvent

* Corresponding author.
E-mail address: nxnghia@iop.vast.vn

https//doi.org/10.25073/2588-1124/vnumap.4769

temperature [8, 9]. Moreover, dual-color emission NCs with enhanced brightness are highly prospective for imaging applications [10]. Previous publications have shown that dual-color emission can be obtained from core/shell/shell nanostructures with the combination of I-type/I-type (CdSe/ZnS/CdSe, PbS/CdS/CdSe [11-15]), quasi-I-type/II-type (CdSe/CdS/ZnSe [16]), and II-type/II-type (PbS/zb-CdSe/wz-CdSe/CdS, PbS/zb-CdS/wz-CdS [17, 18]) carrier trapping modes with zb and wz standing for zinc blende and wurtzite crystal phases respectively, or from transition metal doped NCs (Mn-doped ZnSe/ZnCdSe, Mn-doped CdSSe/ZnS, Mn-doped ZnSe/ZnS/CdS/ZnS, Mn-doped ZnCdSe, Cu- and Mn- co-doped ZnInS [19-23].

In dual-color emission core/shell-type nanoheterostructures, the significant difference in the used materials' lattice constants may result in lattice defects, decreasing their quantum yield. With a small mismatch in the lattice constants of CdSe and CdS (smaller than 3.9% [24]), core/shell-type nanostructures prepared from the two materials are of a way to overcome this disadvantage. In this study, dual-color emissive quantum dot - quantum wells (QDQWs) with core/shell 1/well/shell 2 structure were prepared using one-pot method. The presence of the CdSe core and $CdSe_{1-x}S_x$ alloy well layer with different bandgaps is expected to create two photon types having different energies. The morphology, crystalline structure, vibrational properties, as well as spectroscopic characteristics such as UV-Vis absorption, photoluminescence (PL), and excitation power-dependent and temperature-dependent PL were investigated.

2. Experimental

2.1. Quantum Dot - Quantum well Design

In order to obtain dual-color emission, the QDQWs were designed with a core/shell 1/well/shell 2 structure as described in Figure 1, in which the core and well layers act as emissive domains. The bandgap energy of the well (E_W), shell 1, and shell 2 layers must be larger than that of the core (E_C) to ensure that there is transmission of photons created by radiative recombination inside the core from the nanostructure.

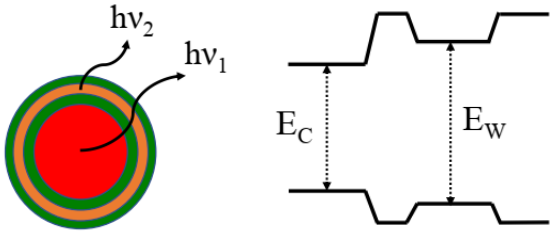

Figure 1. Schematic illustration of the QDQW and energy band diagrams of the nanostructure. E_C and E_W denote the bandgap energies of the core and well, respectively.

The QDQW structure is expected to obtain not only the dual-color emission by radiative recombination in the CdSe core and the $CdSe_{1-x}S_x$ well layer, but also the reduction in Auger recombination, as well as the nanostructure's strain caused by the difference in the lattice constants of CdSe and CdS materials [25-27].

A previous study [28] has shown that the position of the emission peaks and their relative intensities depend not only on the sizes of the core and well layers, but also on the thickness of the shell 1 due to the electronic coupling between the QDQW's 0D and 2D quantum systems. Based on

these results, the dual-color emissive QDQWs have been prepared with shell 1, well layer, and shell 2 thicknesses of 6, 5, and 6 monolayers (MLs), respectively.

2.2. Materials

Initial chemicals including cadmium oxide (CdO, 99.99%), selenium powder (Se, 99.999%), sulfur powder (S, 99.98%), oleic acid (OA, 90%), trioctylphosphine (TOP, 97%), and octadecene (ODE, 90%) were purchased from Sigma Aldrich and used as received, without any further purification.

2.3. Synthesis of the Quantum Dot - quantum Wells

The Se precursor was created by dissolving Se powder in TOP and ODE at 50 ^{o}C, meanwhile the S stock solution was prepared by heating a mixture of S powder and ODE at 80 ^{o}C. The Cd precursor were obtained by dissolving CdO in OA and ODE mixture at 200 ^{o}C. Preparation of the precursor solutions was performed in pure nitrogen gas.

The CdSe/CdS/$CdSe_{1-x}S_x$/CdS QDQW structure was prepared using one-pot method in pure nitrogen gas. The bare-core NCs of a known size were synthesized by quickly injecting the Se precursor solution into the Cd precursor solution flask at 260 ^{o}C, which is then quickly decreased to 220 ^{o}C and maintained for 10 mins for growing the core. It should be noted that the amount of Cd precursor in the reaction flask was calculated for preparing the entire QDQWs. The growth of CdS shell 1 layer on the surfaces of the bare CdSe core was then performed by slowly injecting the S precursor solution into the flask at 220 ^{o}C for 15 min. For the growth of the well and outer shell 2 layers, the Se and S precursor solution mixture and the S precursor solution were added to the reaction flask respectively in the same manner as for the shell 1 layer.

In this work, the bare CdSe core and CdSe/CdS/$CdSe_{1-x}S_x$/CdS QDQW have been taken for the investigation samples. They were isolated from crude solutions by mixing the solutions with isopropanol at a volume ratio of 1:3 and centrifuging with the speed of 14000 rpm for 5 min. The purification process was repeated three times, then the purified NCs were dispersed in toluene.

2.4. Sample Characterization

Transmission electron microscopy (TEM) images of the bare core and QDQW samples were recorded on JEM 1010 microscope (Jeol). Powder X-ray diffraction (XRD) measurements were conducted with the D5005 X-ray diffractometer (Siemens) with Cu-K_α radiation wavelength of 0.15406 nm. UV-Vis absorption spectra were recorded on Varian Cary-5000 spectrometer. To minimize reabsorption, the samples with small amounts of NCs in toluene were used. Raman and photoluminescence (PL) spectra were obtained employing the XploRa Plus spectrometer (Horiba) with laser wavelength of 532 nm. The excitation-power dependent PL measurements were performed for the NCs dispersed in toluene, while the dried NC samples were used for recording temperature-dependent PL spectra. By using Linkam-600 apparatus, the temperature of the samples was varied from 80 K to 300 K. To prevent the laser radiation from heating up the samples, a low excitation power density was used.

3. Results and Discussion

The TEM images of bare core and QDQW samples are shown in Figure 2. The NCs are relatively homogeneous in shape and size. The average size of bare core NCs' is approximately 4.1 nm. As

expected, the formation of the shell 1, well, and shell 2 layers outside the CdSe core has enlarged the QDQWs, reaching an average size of approximately 11 nm.

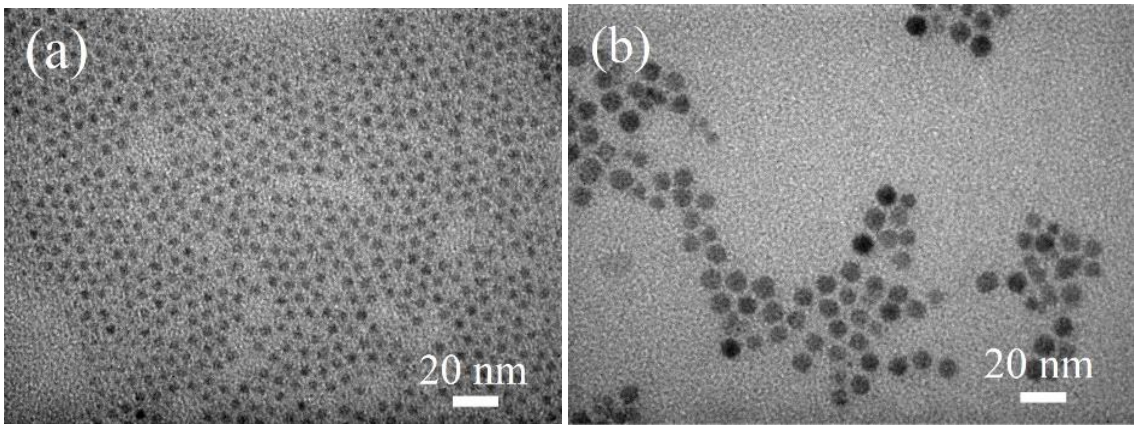

Figure 2. TEM images of the (a) bare core and (b) QDQW samples.

Figure 3a shows the XRD patterns of the bare core and QDQW samples. Their zb structure was confirmed by the existence of diffraction peaks corresponding to Miller indices (111), (220), and (311). In comparison with the bare core's diffraction peaks at 25.4°, 41.9°, and 50°, the positions of the QDQW's peaks are slightly shifted towards larger 2θ angles, namely, at 25.5°, 42.5°, and 50.2°. Since the lattice constant of CdS structure is smaller than that of CdSe, the diffraction peak shift of the QDQW sample is attributed to the superposition of XRD patterns of the core and its surrounding outer layers.

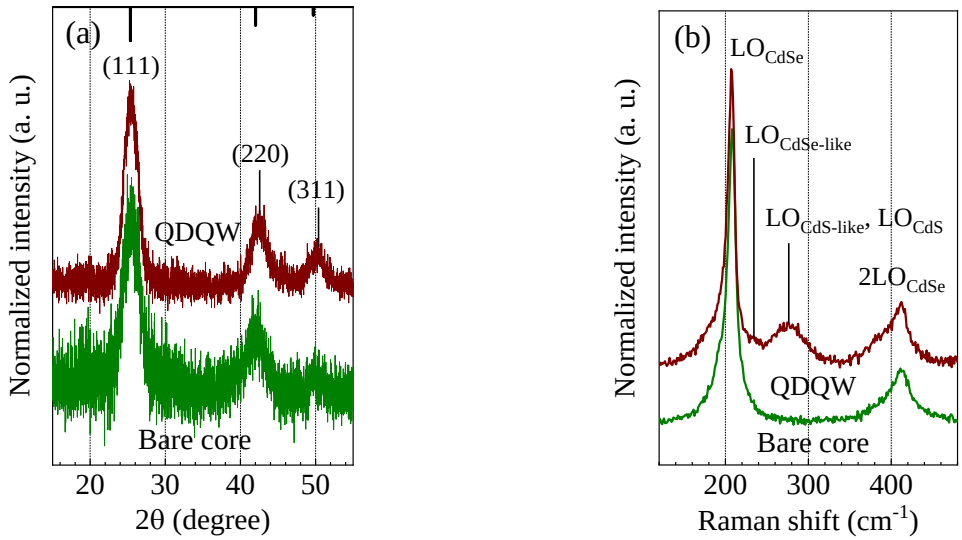

Figure 3. XRD patterns (a) and Raman spectra of the bare core and QDQW (b) samples.

The formation of the CdS/CdSe$_{1-x}$S$_x$/CdS domain surrounding the CdSe core in the QDQW nanostructure can be more clearly identified by comparing the bare core and QDQW samples' Raman

spectra. As seen in Figure 3b, the bare core's Raman spectrum is characterized by Raman peaks centered at 208 and 413 cm^{-1}, which are attributed to the CdSe NC's first - order (LO_{CdSe}) and second - order ($2LO_{CdSe}$) Raman scattering. The formation of shell 1, well, and shell 2 layers surrounding the CdSe core leads to the appearance of a low-intensity $LO_{CdSe\text{-}like}$ Raman peak at approximately 230 cm^{-1} (vibrational mode of the $CdSe_{1-x}S_x$ alloy well layer) and a relatively broad Raman peak at 276 cm^{-1} caused by the superposition of the well's $LO_{CdS\text{-}like}$ and the two shells' LO_{CdS} vibrational modes [29].

Figure 4 is the UV-Vis absorption and PL spectra of the bare core and QDQW samples. The absorption peak's structure can be clearly seen due to the NCs' narrow size distribution. The formation of the $CdS/CdSe_{1-x}S_x/CdS$ domain surrounding the CdSe core causes the red-shift of the first absorption peak from 2.13 to 1.99 eV, and the broadening of the absorption peak at high energy. The bare core sample's PL spectrum includes a near band edge emission peak (P_C) at 2.1 eV and a broad emission band at the lower energy centered at 1.61 eV related to surface states. Similar to the UV-Vis absorption spectrum, the surrounding of the CdSe core by three outer layers caused a red-shift of P_C peak from 2.1 to 1.97 eV, and significantly decreases the low energy side broad emission band. Notably, a new peak at 2.2 eV appears in the QDQW sample's PL spectrum, which is attributed to the radiative recombination in the $CdSe_{1-x}S_x$ well layer (marked as P_W).

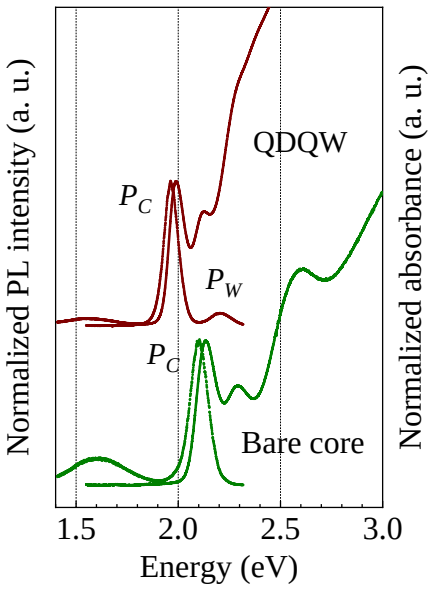

Figure 4. UV-Vis absorption and PL spectra of the bare core and QDQW samples.

The PL spectra of QDQWs dispersed in toluene were measured at room temperature with excitation power densities in the range of $(0.013 - 13)\times10^2$ mW/cm^2 (Figure 5a). As the excitation power density increases, the position and full width at half maximum (FWHM) of the P_C and P_W peaks are insignificantly changed; however, their PL intensities increase. As seen in Figure 5b, the integrated PL intensities of the two peaks (marked as I_C and I_W) as a function of excitation power density show a linear increase in the low power density region up to 1.3×10^2 mW/cm^2. Using the relation of $I \sim \text{Power}^{\gamma}$ [30], the obtained value of γ is approximately 1 for both the P_C and P_W peaks, reflecting the QDQW's emission generated by exciton recombination in the core and well layers. At higher power densities, the integrated PL intensities continue to rise with the power, but the linearity is no longer maintained. Since the QDQWs are dispersed in toluene, thermal effect can be ruled out in the

measurement. When the integrated PL intensity and lifetime measurements are combined, Peng et al. have pointed out that the linear dependence of integrated PL intensity on excitation power is determined by the excitation intensity, as well as the QDQW's radiative lifetime [31].

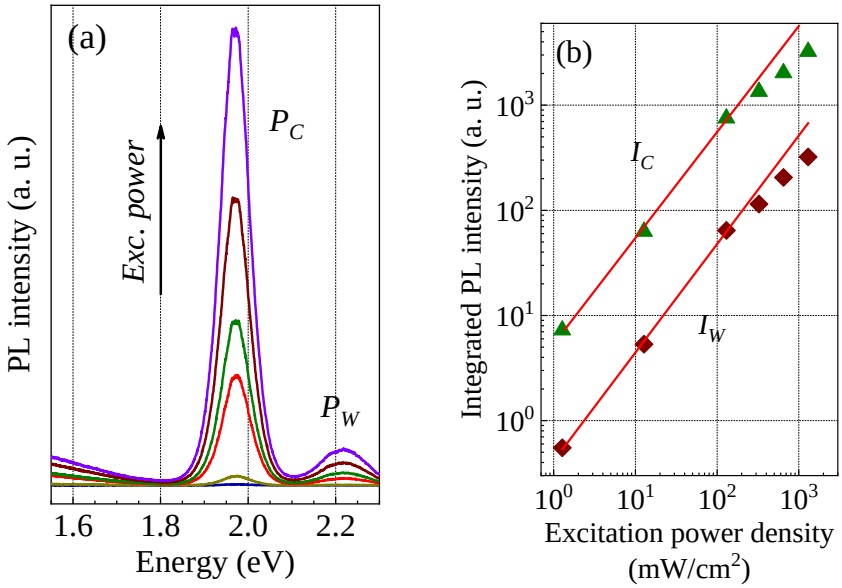

Figure 5. Excitation-power dependent PL spectra of the QDQW sample (a) and Integrated PL intensities of the P_C and P_W peaks as a function of excitation power density (b).

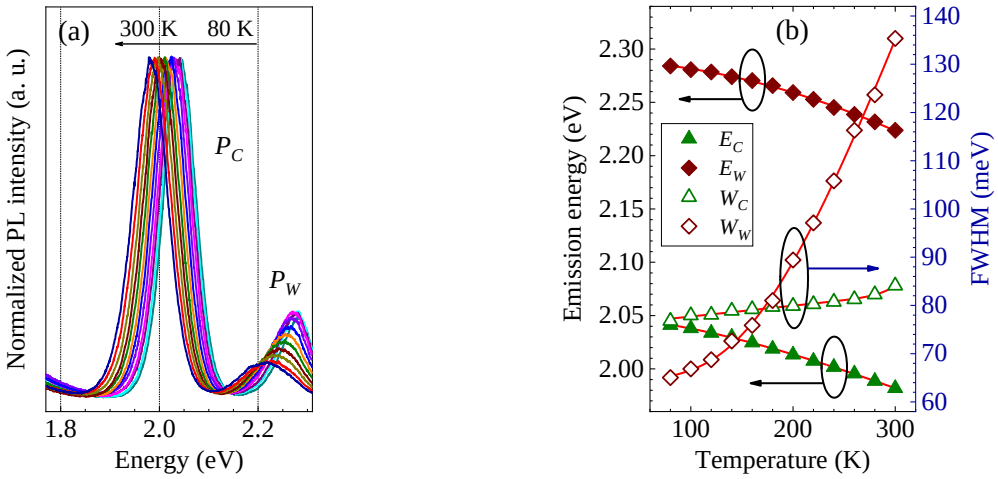

Figure 6. Temperature-dependent PL spectra of the QDQW sample (a) and Energy positions and FWHMs of the P_C and P_W peaks as a function of temperature (b).

The temperature-dependent of PL spectra of QDQW in a temperature range of 80 - 300 K are shown in Figure 6a. As temperature increases, the PL peak is shifted towards lower energy. The

temperature-dependent shift of the P_C and P_W peaks can be attributed to the lattice dilation and electron-phonon interaction as described in the Varshni expression [32, 33]:

$$E(T)=E(0)-\alpha T^2/(\beta+T)$$

where *E(0)* is the bandgap energy at 0 K, α is the temperature coefficient, and β is expected to be comparable with the material's Debye temperature.

As shown in Figure 6b, the emission energies are well fitted with the Varshni expression. The *E(0)*, α, and β parameters obtained from fitting of the energy positions of emission peaks are respectively 2.048 eV, 4.9 × 10^{-4} eV/K, and 357 K for P_C peak, and 2.289 eV, 2.8 × 10^{-3} eV/K, and 3448 K for P_W peak. Figure 6b indicates that the peaks' FWHMs change differently as the temperature increases. The FWHM of P_C peak changes from 76 to 84 meV, while that of P_W peak changes significantly from 65 to 135 meV when the temperature increases from 80 to 300 K.

Observation of the change of the P_W peak by temperature in detail reveals the appearance of a new emission peak at approximately 2.18 eV whose intensity increases with temperature (Figure 7), causing a strong shift and a broadening of the P_W peak towards the lower energy. This explains why the relatively larger α, β fitting parameter values and the more rapid increase of FWHM with temperature for the P_W peak were obtained in comparison with those for the P_C peak. As known, "local wells" with different depths can be created in the QDQW's well layer by the random distribution of chemical elements in ternary and quarternary semiconductor compounds [34] and/or the rough well/shell interface caused by the Stranski-Krastanov growth mechanism [35]. The rise in temperature increasing the number of free carriers in the well layer's "local wells" causes the emission peak at 2.18 eV appeared.

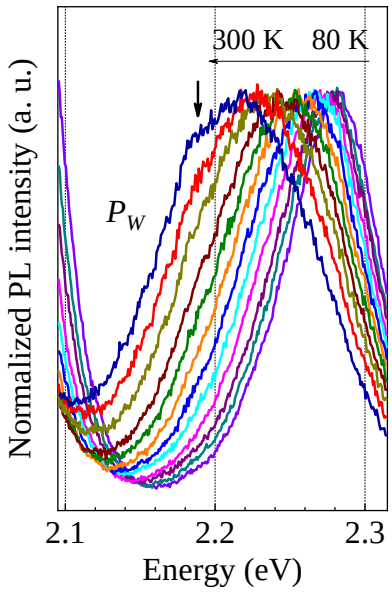

Figure 7. Change of the P_W peak vs temperature.

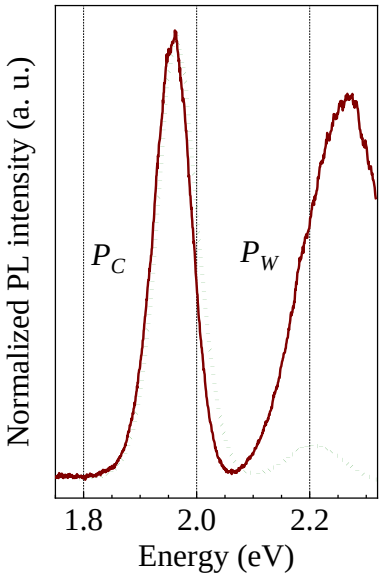

Figure 8. Comparison of PL spectra of non-annealed and annealed QDQW samples (shown in dotted and solid lines respectively).

As shown in Figure 4, the relative intensity of the P_W peak is lower than that of the P_C peak (I_W/I_C ~ 8 %). Annealing QDQW samples in the reaction solution for 45 min made the I_W/I_C ratio increase up to 85 % (Figure 8). This indicates how important role the interface quality in the QDQW structure plays in its emission efficiency.

4. Conclusion

In summary, CdSe/CdS/$CdSe_{1-x}S_x$/CdS QDQW structure was prepared by the colloidal method and its spectroscopic characteristics were investigated. The QDQWs have a zinc blende structure with an average diameter of 11 nm. The creation of the CdSe/CdS/$CdSe_{1-x}S_x$/CdS structures was confirmed by Raman spectroscopy. PL spectra, as a function of excitation power, show a linear relationship at low excitation intensity and a nonlinear behavior as the excitation intensity increases. The temperature dependence of the bandgap energies of the CdSe core and $CdSe_{1-x}S_x$ well has been analyzed with the Varshni relation. The relatively larger values of the α temperature coefficient, β Debye temperature, and the rapid increase of FWHM with temperature for the P_W peak in comparison with those for the P_C peak were explained due to the existence of the "local wells" in the well layer of the QDQW structure. The emission efficiency of the well layers was significantly increased by the samples annealing.

Acknowledgements

The present research is funded by International Center of Physics under grant number ICP.2021.09.

Credit Authorship Contribution Statement

Le Anh Thi, Nguyen Dieu Linh, Le Duc Huy: Conceptualization, Investigation, Data curation, Writing-original draft. Nguyen Thi Thuy Lieu: Methodology, Formal analysis, Funding acquisition. Nguyen Thi Minh Hien: Validation, Writing-review & editing. Nguyen Xuan Nghia: Supervision, Writing-review & editing.

Declaration of Competing Interest

The authors declare that they have no known competing financial interests or personal relationships that could have appeared to influence the work reported in this paper.

References

[1] H. Deng, J. Liu, H. Zhang, C. Li, Z. Liu, D. Che, Dual-color Fluorescence Imaging and Magnetic Resonance Imaging of Gd_2O_3:Dy^{3+} Nanoparticles Synthesized by Laser Ablation in Water, J. Mater. Sci.: Mater. Electron, Vol. 32, 2021, pp. 14932-14943, https://doi.org/10.1007/s10854-021-06045-8.

[2] A. Forder, S. A. Thomas, R. J. Petersen, S. L. Brown, D. S. Kilin, E. K. Hobbie, Size Dependent Doping Synergy and Dual-Color Emission in $CsPb_{1-x}Mn_xCl_3$ Nanocrystals, J. Phys. Chem. C, Vol. 125, 2021, pp. 18849-18856, https://doi.org/10.1021/acs.jpcc.1c06995.

[3] X. Yang, X. Liu, B. Gu, H. Liu, R. Xiao, C. Wang, S. Wang, Quantitative and Simultaneous Detection of Two Inflammation Biomarkers Via A Fluorescent Lateral Flow Immunoassay Using Dual-color SiO_2@QD Nanotags, Microchim. Acta, Vol. 187, 2020, pp. 570(1)-570(11), https://doi.org/10.1007/s00604-020-04555-6.

[4] S. Chen, Y. Hong, Y. Liu, J. Liu, C. W. T. Leung, M. Li, R. T. K. Kwok, E. Zhao, J. W. Y. Lam, Y. Yu, B. Z. Tang, Full-Range Intracellular pH Sensing by an Aggregation - Induced Emission-Active Two-Channel Ratiometric Fluorogen, J. Am. Chem. Soc., Vol. 135, 2013, pp. 4926-4929, https://doi.org/10.1021/ja400337p.

[5] A. M. Dennis, W. J. Rhee, D. Sotto, S. N. Dublin, G. Bao, Quantum Dot-Fluorescent Protein FRET Probes for Sensing Intracellular pH, ACS Nano, Vol. 6, 2012, pp. 2917-2924, https://doi.org/10.1021/nn2038077.

[6] I. L. Medintz, M. H. Stewart, S. A. Trammell, K. Susumu, J. B. Delehanty, B. C. Mei, J. S. Melinger, J. B. B. Canosa, P. E. Dawson, H. Mattoussi, Quantumdot/Dopamine Bioconjugates Function as Redox Coupled Assemblies for in Vitro and Intracellular pH Sensing, Nat. Mater., Vol. 9, 2010, pp. 676-684, https://doi.org/10.1038/nmat2811.

[7] M. Lorenzon, V. Pinchetti, F. Bruni, W. K. Bae, F. Meinardi, V. I. Klimov, S. Brovelli, Single-Particle Ratiometric Pressure Sensing Based on Double-Sensor Colloidal Nanocrystals, Nano Lett., Vol. 17, 2017, pp. 1071-1081, https://doi.org/10.1021/acs.nanolett.6b04577.

[8] E. J. McLaurin, V. A. Vlaskin, D. R. Gamelin, Water-Soluble Dual-Emitting Nanocrystals for Ratiometric Optical Thermometry, J. Am. Chem. Soc., Vol. 133, 2011, pp. 14978-14980, https://doi.org/10.1021/ja206956t.

[9] A. E. Albers, E. M. Chan, P. M. McBride, C. M. A. Franklin, B. E. Cohen, B. A. Helms, Dual-Emitting Quantum Dot/Quantum Rod-Based Nanothermometers with Enhanced Response and Sensitivity in Live Cells, J. Am. Chem. Soc., Vol. 134, 2012, pp. 9565-9568, https://doi.org/10.1021/ja302290e.

[10] E. A. Dias, A. F. Grimes, D. S. English, P. Kambhampati, Single Dot Spectroscopy of Two-Color Quantum Dot/Quantum Shell Nanostructures, J. Phys. Chem. C, Vol. 112, 2008, pp. 14229-14232, https://doi.org/10.1021/jp806621q.

[11] E. A. Dias, J. I. Saari, P. Tyagi, P. Kambhampati, Improving Optical Gain Performance in Semiconductor Quantum Dots Via Coupled Quantum Shells, J. Phys. Chem. C, Vol. 116, 2012, pp. 5407-5413, https://doi.org/10.1021/jp211325x.

[12] E. A. Dias, S. L. Sewall, P. Kambhampati, Light Harvesting and Carrier Transport in Core/Barrier/Shell Semiconductor Nanocrystals, J. Phys. Chem. C, Vol. 111, 2007, pp. 708-713, https://doi.org/10.1021/jp0658389.

[13] E. A. Dias, A. F. Grimes, D. S. English, P. Kambhampati, Single Dot Spectroscopy of Two-color Quantum Dot/Quantum Shell Nanostructures, J. Phys. Chem. C, Vol. 112, 2008, pp. 14229-14232, https://doi.org/10.1021/jp806621q.

[14] D. Battaglia, B. Blackman, X. Peng, Coupled and Decoupled Dual Quantum Systems in One Semiconductor Nanocrystal, J. Am. Chem. Soc., Vol. 127, 2005, pp. 10889-10897, https://doi.org/10.1021/ja0437297.

[15] N. Razgoniaeva, M. R. Yang, C. Colegrove, N. Kholmicheva, P. Moroz, H. Eckard, A. Vore, M. Zamkov, Double-Well Colloidal Nanocrystals Featuring Two-color Photoluminescence, Chem. Mater., Vol. 29, 2017, pp. 7852-7858. https://doi.org/10.1021/acs.chemmater.7b02585.

[16] U. Soni, A. Pal, S. Singh, M. Mittal, S. Yadav, R. Elangovan, S. Sapra, Simultaneous Type-I/type-II Emission from CdSe/CdS/ZnSe Nano-heterostructures, ACS Nano, Vol. 8, 2014, pp. 113-123, https://doi.org/10.1021/nn404537s.

[17] A. Teitelboim, D. Oron, Broadband Near-Infrared to Visible Upconversion in Quantum Dot-Quantum Well Heterostructures, ACS Nano, Vol. 10, 2016, pp. 446-452, https://doi.org/10.1021/acsnano.5b05329.

[18] H. Zhao, G. Sirigu, A. Parisini, A. Camellini, G. Nicotra, F. Rosei, V. Morandi, M. Zavelani-Rossi, A. Vomiero, Dual Emission in Asymmetric 'Giant' PbS/CdS/CdS Core/Shell/Shell Quantum Dots, Nanoscale, Vol. 8, 2016, pp. 4217-4226, https://doi.org/10.1039/C5NR08881J.

[19] V. A. Vlaskin, N. Janssen, J. V. Rijssel, R. Beaulac, D. R. Gamelin, Tunable Dual Emission in Doped Semiconductor Nanocrystals, Nano Lett., Vol. 10, 2010, pp. 3670-3674. https://doi.org/10.1021/nl102135k.

[20] C. H. Hsia, A. Wuttig, H. Yang, An Accessible Approach to Preparing Water-Soluble Mn^{2+}-Doped (Cdsse)Zns (Core) Shell Nanocrystals for Ratiometric Temperature Sensing, ACS Nano, Vol. 5, 2011, pp. 9511-9522, https://doi.org/10.1021/nn2025622.

[21] E. J. McLaurin, V. A. Vlaskin, D. R. Gamelin, Watersoluble Dual-emitting Nanocrystals for Ratiometric Optical Thermometry, J. Am. Chem. Soc., Vol. 133, 2011, pp. 14978-14980, https://doi.org/10.1021/ja206956t.

[22] E. J. McLaurin, M. S. Fataftah, D. R. Gamelin, One-step Synthesis of Alloyed Dualemitting Semiconductor Nanocrystals, Chem. Commun., Vol. 49, 2013, pp. 39-41, https://doi.org/10.1039/C2CC36862E.

[23] S. Cao, J. J. Zheng, J. L. Zhao, Z. B. Yang, M. H. Shang, C. M. Li, W. Y. Yang, X. S. Fang, Robust and Stable Ratiometric Temperature Sensor Based on Zn-In-S Quantum Dots with Intrinsic Dual-dopant Ion Emissions, Adv. Funct. Mater., Vol. 26, 2016, pp. 7224-7233, https://doi.org/10.1002/adfm.201603201.

[24] J. V. Embden, J. Jasieniak, D. E. Gómez, A. P. Mulvaney, M. Giersig, Review of the Synthetic Chemistry Involved in the Production of Core/Shell Semiconductor Nanocrystals, Aust. J. Chem., Vol. 60, 2007, pp. 457-471, https://doi.org/10.1071/CH07046.

[25] D. V. Talapin, I. Mekis, S. Go1tzinger, A. Kornowski, O. Benson, H. Weller, CdSe/CdS/ZnS and CdSe/ZnSe/ZnS Core-Shell-Shell Nanocrystals, J. Phys. Chem. B, Vol. 108, 2004, pp. 18826-18831, https://doi.org/10.1021/jp046481g.

[26] R. Xie, U. Kolb, J. Li, T. Basche, A. Mews, Synthesis and Characterization of Highly Luminescent CdSe-Core CdS/$Zn_{0.5}Cd_{0.5}$S/ZnS Multishell Nanocrystals, J. Am. Chem. Soc., Vol. 127, 2005, pp. 7480-7488, https://doi.org/10.1021/ja042939g.

[27] S. Jun, E. Jang, J.E. Lim, Synthesis of Multi-shell Nanocrystals by A Single Step Coating Process, Nanotechnology, Vol. 17, 2006, pp. 3892-3896, https://doi.org/10.1088/0957-4484.

[28] D. Battaglia, B. Blackman, X. Peng, Coupled and Decoupled Dual Quantum Systems in One Semiconductor Nanocrystal, J. Am. Chem. Soc., Vol. 127, 2005, pp. 10889-10897, https://doi.org/10.1021/ja0437297.

[29] A. Roy, A. K. Sood, Surface and Confined Optical Phonons in CdS_xSe_{1-x} Nanoparticles in A Glass Matrix, Phys. Rev. B, Vol. 53, 1996, pp. 12127-12132, https://doi.org/10.1103/PhysRevB.53.12127.

[30] A. G. Joly, W. Chen, D. E. McCready, J. O. Malm, J. O. Bovin, Upconversion Luminescence of CdTe Nanoparticles, Phys. Rev. B, Vol. 71, 2005, pp. 165304(1)-165304(9), https://doi.org/10.1103/PhysRevB.71.165304.

[31] D. Battaglia, B. Blackman, X. Peng, Coupled and Decoupled Dual Quantum Systems in One Semiconductor Nanocrystal, J. Am. Chem. Soc., Vol. 127, 2005, pp. 10889-10897, https://doi.org/10.1021/ja0437297.

[32] D. Valerini, A. Cretí, M. Lomascolo, L. Manna, R. Cingolani, M. Anni, Temperature Dependence of the Photoluminescence Properties of Colloidal Cdse/Zns Core/Shell Quantum Dots Embedded in A Polystyrene Matrix, Phys. Rev. B, Vol. 71, 2005, pp. 235409(1)- 235409(6), https://doi.org/10.1103/PhysRevB.71.235409.

[33] J. Xu, D. Battaglia, X. Peng, M. Xiao, Photoluminescence from Colloidal CdS-CdSe-CdS Quantum Wells, J. Opt. Soc. Am. B, Vol. 22, 2005, pp.1112-1116, https://doi.org/10.1364/JOSAB.22.001112.

[34] E. F. Schubert, E. O. Gobel, Y. Horikoshi, K. Ploog, H. J. Queisser, Alloy Broadening in Photolurninescence Spectra of $Al_xGal_{1-x}As$, Phys. Rev. B, Vol. 30, 1984, pp. 813-820, https://doi.org/10.1103/PhysRevB.30.813.

[35] Z. J. Jiang, D. F. Kelley, Stranski-Krastanov Shell Growth in ZnTe/CdSe Core/Shell Nanocrystals, J. Phys. Chem. C, Vol. 117, 2013, pp. 6826-6834, https://doi.org/10.1021/jp4002753.